



Effect of Pressure on Electronic, Mechanical and Dynamic Properties for Orthorhombic WP

Ceren TAYRAN^{1,*} , Mehmet CAKMAK^{2,3} 

¹Gazi University, Faculty of Science, Department of Physics, 06500, Ankara, Turkey

²Gazi University, Faculty of Applied Sciences, Department of Photonics, 06500, Ankara, Turkey

³Gazi University, Photonics Application and Research Center, 06500, Ankara, Turkey

Highlights

- The electronic band structure of WP shows metallic behavior under pressure.
- WP remains mechanically stable and elastically ductile under pressure.
- The metallic structure of WP is preserved with increasing pressure.
- WP is dynamically stable under pressure.

Article Info

Received: 29 May 2022

Accepted: 19 Sep 2022

Keywords

DFT

Electronic and
Mechanical properties
Phonon dispersions

Abstract

The structural, mechanical, electronic and dynamic features of MnP-type WP have been presented under 0-50 GPa hydrostatic pressure utilizing density functional theory. The lattice constants, values of volumes and bond lengths have been decreased with increasing pressure. It has been found that results of electronic band structures show that WP preserves its metallic feature under pressure. It has been observed that electronic band structures shifted up in $Y-\Gamma$ and $\Gamma-X$ symmetry points under pressure. The partial density of states indicates that hybridization occurs between W-d and P-p orbitals and also W-d orbital is dominated at all pressures. It is obtained that the mechanical properties of WP are increased with increasing pressure. Additionally, WP becomes more ductile under pressure. According to phonon dispersions, it has been investigated that WP is dynamically stable under pressure applied.

1. INTRODUCTION

CrAs, MnP, FeP, CoP, RuP, IrP and WP compounds with MnP-type (B31) structures are attracting attention due to their special properties such as superconductivity and competing phenomena, photochemical cells, and advantage in photoelectrodes in chargeable solar batteries [1-8]. This structure is defined by the formula MX (M represents the transition metal and X represents Sb, As and P atoms) [8-14]. MX compounds crystallize orthorhombic MnP-type or the hexagonal NiAs-type structure [8, 15]. WP has much more attention because of it is a 5d-transition metal [8]. Indeed, 5d-transition metal electrons are freely moving, so no magnetic ordering is observed [16]. This importance is necessary for understanding the connection between ambient pressure and superconductivity in MnP-type compounds.

WP is an orthorhombic MnP-type structure [17-19]. Faller et al. [20] studied Mo-P and W-P systems using tensimetric and X-ray powder methods. As a result, Mo₃P, MoP, MoP₂, WP and WP₂ phases were obtained. They found that WP is in an MnP-type structure. However, they did not give unit cell dimensions. According to this, Schönberg [21] and Bachmayer et al. [22] proposed unit cell dimensions. Rundqvist et al. [2] studied Mo-P and W-P systems using X-ray powder methods. They reported orthorhombic unitcell dimensions for WP compound and some extra physical information. Gopalakrishnan et al. [23] synthesized transition-metal phosphides (FeP, RuP, WP, MoP, Ni₂P, Fe₂P), arsenides (CoAs, NiAs), and antimonides (CoSb₃, NiSb₂) using hydrogen reduction. One of the experimental studies was done by Lesnyak et al. [24]. They synthesized AlP, CrP, NbP, MoP and WP using lithium metaphosphate LiPO₃. They reported the

*Corresponding Author, e-mail: c.tayran@gazi.edu.tr

thermodynamic parameters of the reactions and the temperature modes of these compounds. A theoretical study done by Jaiganesh et al. [25] also obtained the fundamental physical properties of group V compounds such as MoP, MoBi, MoSb, WSb and WN. In the study by Joshi et al. [3], momentum densities for WP and MoP compounds were investigated with BPBE-GGA and second-order (SO) GGA-PBE functional. In this study, obtained results were compared with existing theoretical and experimental electronic energy band structures, the density of states and as well as Mulliken population analysis. It has been shown that the SO-GGA-PBE-based profiles have the best results. Recently, WP material has attracted much attention with new studies. On the experimental side, superconductivity in WP single crystals at ambient pressure has been reported in literature by Liu et al. [8]. They have found that the electrical resistivity, specific heat, and ac magnetic susceptibility have showed bulk superconductivity of $T_c \sim 0.8$ K. The interest of WP has been reported that the superconductivity is dominated by the 5d-orbital. They have suggested that WP compound indicates a weak-coupling Bardeen-Cooper-Schrieffer (BCS) superconductor. On the theoretical side, WP's mechanical, electronic and especially superconducting properties have been calculated using DFT [26]. Indeed, 5d-orbital for WP has characterized the superconductivity and electronic structure. Furthermore, WP's structural and electronic properties as well as CrAs and MnP compounds have been studied using DFT with an effective low-energy model Hamiltonian [9].

The physical properties of crystals with changes in pressure are important in understanding the deformation behavior that occurs with compression in materials. Besides, this behavior ensures analyzing the nature of the solid-state. Examining the effect of changing pressure on various properties of the material is a crucial way to interpret the changes that may observe in the physical and chemical properties of the material. In our study, the first-principle calculations have been used to understand the influence of pressure on the structural, mechanical, electronic and dynamical properties of WP compound to fill the empty part of the WP puzzle about the pressure characteristics in literature. The lattice and elastic constants, Bulk modulus, Shear modulus, Young's modulus, brittle/ductile behavior and hardness of the compound have been studied over 0-50 GPa hydrostatic pressure range. The results indicate that WP is mechanically stable with increasing pressure. The electronic properties are studied to analyze electrical and actual bonding states. In addition, the pressure dependence of the distributions for phonon density and partial phonon density is calculated. According to this calculation, WP remained dynamically stable with increasing pressure values.

2. MATERIAL METHOD

All our calculations have been done using the Vienna ab initio simulation package program (VASP) [27-29] built on density functional theory (DFT) and taking into account the exchange-correlation energies with the generalized gradient approach (GGA) of Perdew Burke Ernzerhof (PBE) scheme [30]. To characterize the electron-ion interactions, projector-augmented waves (PAW) [31, 32] were employed. k-point mesh was considered a grid of $8 \times 14 \times 8$ Monkhorst-Pack [33]. Cutoff energy was used to 500 eV. The energy and Hellmann-Feynman force criteria were adjusted to 1.0×10^{-6} eV and less than 1.0×10^{-4} eV/Å, respectively. $6s^2 5d^4$ for W and $3s^2 3p^3$ for P electron states have been treated as valence electrons. The crystal structure was depicted by VESTA [34]. The PHONOPY package [35] was used to investigate the dynamic stability of WP at different pressure values.

3. THE RESEARCH FINDINGS AND DISCUSSION

MnP-type WP crystallizes in the orthorhombic structure as given in Figure 1(a) (*Pnma* (62) space group) [17-19] and the first Brillouin zone is plotted with high symmetry points as seen in Figure 1(b). The primitive cell contains 4 W atoms and 4 P atoms. The values of lattice constant and volume obtained in our study at 0 GPa and under different pressure are written in Tables 1, 2 and 3, respectively. Besides, the experimental [1, 2, 17, 23, 24] and theoretical [3, 8, 25, 26] values are also given in Table 1 to compare and check our results. For better illustration, the graph of variation of normalized lattice constants represented by a/a_0 , b/b_0 , and c/c_0 with increasing pressure is shown in Figure 3(a). The obtained results indicate that when the pressure is increased, lattice parameters decrease. The b/b_0 ratio decreases a little faster a/a_0 and c/c_0 , respectively. The obtained lattice constants in our study are compatible with the available experimental and theoretical values at 0 GPa. This result indicates that WP has a stronger stiffness along the b-axis than another axis. In previous studies [15, 36, 37], it has been reported that b-axis length

decreases with increasing pressure for CrAs and CrP structures. It is known that CrAs, CrP, and WP are MnP type (B31) structures. Therefore, calculated values of b -axis length are compatible with the previous results for MnP type structures. Additionally, we have calculated four inequivalent values of bond lengths between W and P atoms (d_{W-P_1} , d_{W-P_2} , d_{W-P_3} , d_{W-P_4}) at 0 GPa as indicated in Figure 1(a) and listed in Table 2. Besides, available theoretical [9] and experimental [17] results are given in Table 2. Our calculations are compatible with these values at 0 GPa. We have also given bond lengths under pressure in Table 3. As can be seen from our results, W-P bond lengths have decreased with pressure enhanced.

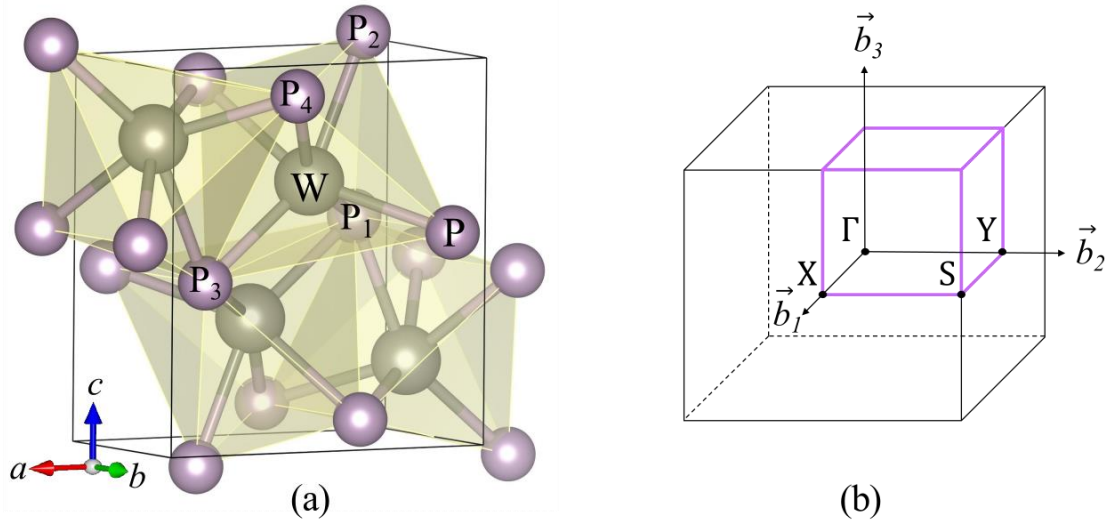


Figure 1. (a) The primitive cell of the orthorhombic WP crystal structure and (b) the Brillouin zone

Table 1. The equilibrium lattice constants a, b, c (Å), and volume V (Å³) of WP with experimental and theoretical values at the ambient pressure

	a	b	c	V
This Work	5.743	3.261	6.247	117.000
Experimental [1]	5.734	3.249	6.222	115.900
Experimental [2]	5.732	3.249	6.222	
Experimental [17]	5.731	3.248	6.227	
Experimental [23]	5.729	3.250	6.220	
Experimental [24]	5.780	3.240	6.290	115.870
Theoretical [3]	5.731	3.248	6.227	
Theoretical [8]	5.722	3.243	6.211	115.270
Theoretical [25]	5.768	3.269	6.267	
Theoretical [26]	5.743	3.261	6.247	117.000

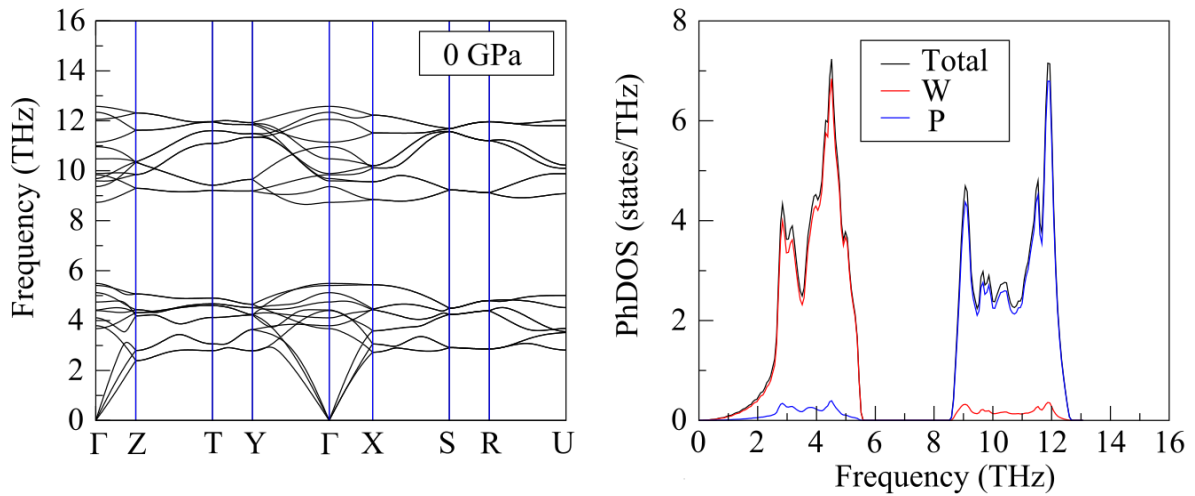
Table 2. The equilibrium bond lengths d_{W-P_1} , d_{W-P_2} , d_{W-P_3} , d_{W-P_4} (Å) (as shown in Figure 1(a)) of WP with experimental and theoretical values at the ambient pressure

	d_{W-P_1}	d_{W-P_2}	d_{W-P_3}	d_{W-P_4}
This Work	2.503	2.554	2.472	2.511
Theoretical [9]	2.497	2.534	2.465	2.497
Experimental [17]	2.497	2.538	2.468	2.504

Table 3. The equilibrium lattice constants a, b, c (\AA), volume V (\AA^3) and bond lengths d_{W-P_1} , d_{W-P_2} , d_{W-P_3} , d_{W-P_4} (\AA) (as shown in Figure 1(a)) of WP over (0–50) GPa pressure range

Pressure (GPa)	a	b	c	V	d_{W-P_1}	d_{W-P_2}	d_{W-P_3}	d_{W-P_4}
0	5.743	3.261	6.247	117.000	2.503	2.554	2.472	2.511
10	5.659	3.196	6.209	112.320	2.484	2.514	2.451	2.474
20	5.590	3.142	6.178	108.510	2.466	2.483	2.432	2.446
30	5.531	3.095	6.151	105.300	2.500	2.457	2.414	2.422
40	5.480	3.053	6.128	102.520	2.435	2.435	2.398	2.402
50	5.434	3.015	6.107	100.070	2.421	2.416	2.383	2.384

We have computed the phonon dispersions and phonon density of states of the WP compound under different pressures to find out dynamic stability. The calculated phonon dispersion curves are drawn in Figure 2. The primitive cell of the WP compound contains eight atoms; therefore, there are twenty-four phonon branches which consist of three acoustics and twenty-one optical branches. Figures 2(a) and (b) show positive phonon frequencies for 0 GPa and 50 GPa. WP is dynamically stable with increasing pressure without any imaginary phonon frequencies. We can also see gaps between the optical and acoustic modes due to the difference in the atomic masses between W and P atoms. The gap between the optical and acoustic phonons branches increases with increasing pressure. As far as we know, there is no experimental data other than our previous theoretical study [26].



(a)

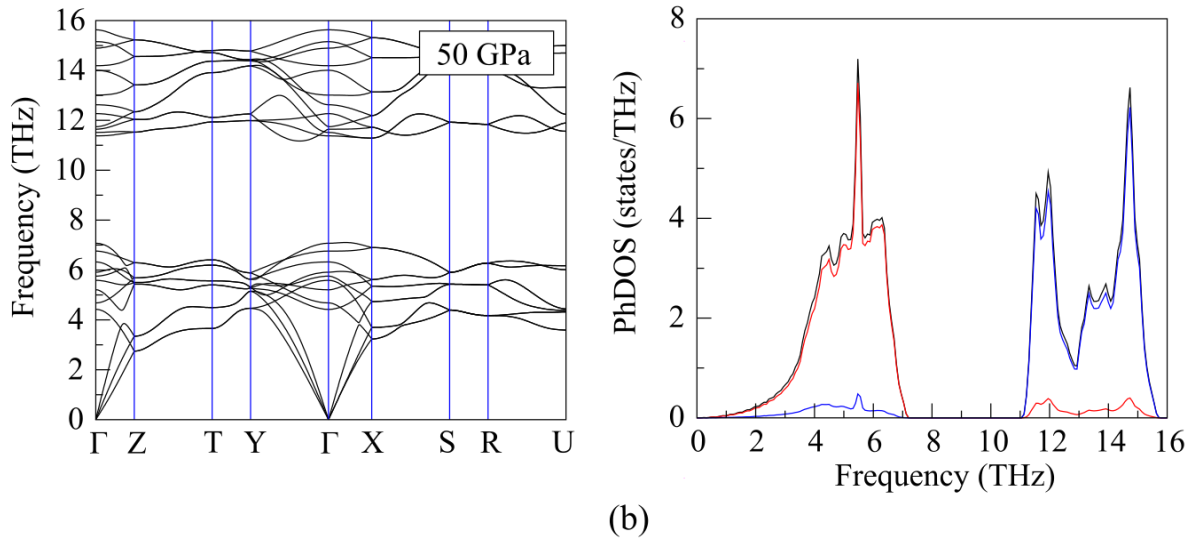


Figure 2. The calculated pressure-dependent phonon dispersion, phonon total, and partial-projected density of states for WP at (a) 0 Gpa, and (b) 50 Gpa

Furthermore, we have examined both elastic constants and mechanical behavior of WP compound under pressure. The elastic constants are have been evaluated using the stress-strain method [38] for analyzing the resisting ability of deformation under external pressure [39]. The nine independent elastic constants defined for an orthorhombic crystal structure are indicated as C_{11} , C_{22} , C_{33} , C_{44} , C_{55} , C_{66} , C_{12} , C_{13} and C_{23} , and these must satisfy the following relations for the mechanical stability [40-46]:

$$\begin{aligned} \tilde{C}_{ii} &> 0, \quad (i = 1, 2, \dots, 6) \\ [\tilde{C}_{11} + \tilde{C}_{22} + \tilde{C}_{33} + 2(\tilde{C}_{12} + \tilde{C}_{13} + \tilde{C}_{23})] &> 0, \\ (\tilde{C}_{11} + \tilde{C}_{22} - 2\tilde{C}_{12}) &> 0, \\ (\tilde{C}_{11} + \tilde{C}_{33} - 2\tilde{C}_{13}) &> 0, \\ (\tilde{C}_{22} + \tilde{C}_{33} - 2\tilde{C}_{23}) &> 0 \end{aligned}$$

where $\tilde{C}_{ii} = C_{ii} - P$, $\tilde{C}_{12} = C_{12} + P$, $\tilde{C}_{13} = C_{13} + P$, $\tilde{C}_{23} = C_{23} + P$. We have also calculated elastic constants as listed in Table 4, which are perfectly matched with the current theoretical results. To understand how pressure will change the elastic constants, the variation of elastic constants with pressure is plotted in Figure 3(b). They are all satisfied with the above formulas on the pressure range of (0-50) GPa; hence WP is mechanically stable in this range. Additionally, the graph of variation of the calculated normalized elastic constants according to the increasing pressure in 10 GPa steps is drawn in Figure 3(b). It is observed that the elastic constants increase as the applied pressure increases. The results found in this study are compatible with the values given in previous theoretical studies [26, 47, 48], as seen in Table 4. Among our results, C_{23} has the highest deviation under pressure. It is also concluded that the value of C_{33} has larger than other elastic constants with all considering pressures. Following the order of elastic constants to pressure are $C_{33} > C_{11} > C_{22} > C_{13} > C_{23} > C_{66} > C_{44} > C_{12} > C_{55}$. Upon this given ranking, C_{11} , C_{22} , and C_{33} represent larger resistance to deformation along the a-, b-, and c-axes, respectively. According to our calculated values, C_{33} is higher than C_{11} at the same pressure. It means that compression applied along the c-axis is more complicated than applying it along the a-axis.

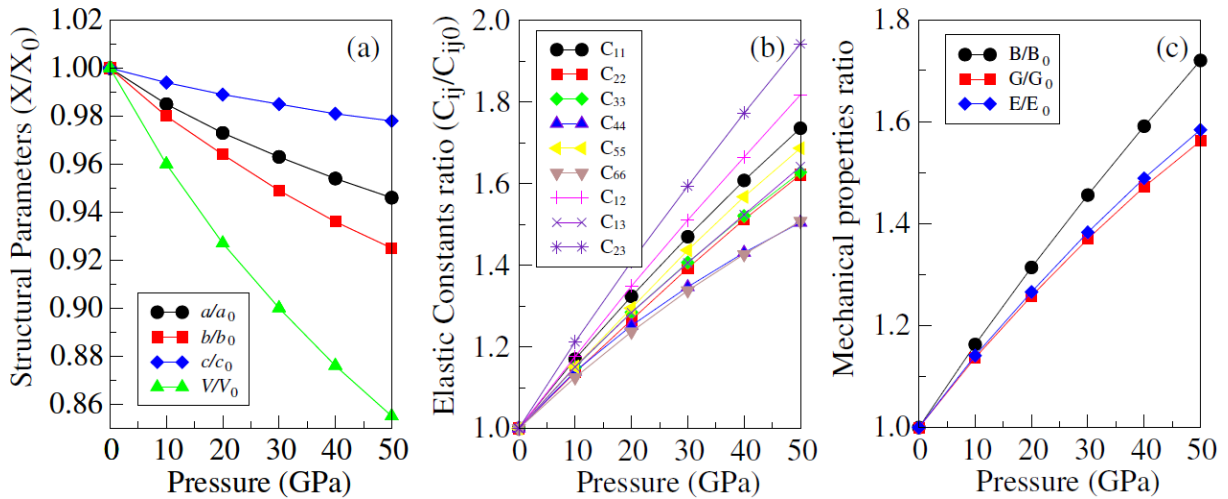


Figure 3. The equilibrium normalized (a) lattice constants a/a_0 , b/b_0 , and c/c_0 , (b) elastic constants C_{ij}/C_{ij0} , and (c) mechanical properties B/B_0 , G/G_0 , and E/E_0 of WP under pressure range 0-50 GPa

Table 4. The equilibrium C_{ij} (GPa) of WP under pressure with previous theoretical values at 0 GPa

Pressure (Gpa)	C_{11}	C_{22}	C_{33}	C_{44}	C_{55}	C_{66}	C_{12}	C_{13}	C_{23}
0	355.71	310.30	461.94	153.30	96.05	176.84	132.17	208.33	162.12
0 (The.) [26]	355.71	310.30	461.94	153.30	96.05	176.84	132.17	208.33	162.12
0 (Theo.)[47, 48]	338.00	311.0	450.00	143.00	90.00	167.00	120.00	203.00	153.00
10	416.31	352.68	531.41	174.69	110.60	199.03	155.45	239.75	196.57
20	470.99	392.99	593.41	191.88	124.39	218.82	178.30	267.45	228.41
30	522.87	432.23	650.07	206.52	138.02	236.55	199.75	292.86	258.49
40	571.81	469.19	702.50	219.35	150.60	252.41	220.03	317.57	287.38
50	617.50	503.16	751.88	230.64	162.01	266.73	240.23	342.10	314.92

It is well known that Bulk modulus (B), shear modulus (G), Young's modulus (E), Poisson's ratio (ν), and B/G ratio are the most common mechanical properties estimated using single-crystal elastic constants. To analyze mechanical characterization, Bulk modulus and Shear modulus are computed using elastic constants C_{ij} , taking into account the Voigt-Reuss-Hill approximations (VRH). The Voigt approximation (V) [49] and Reuss approximation (R) [50] provide the theoretical upper limit and lower limit of the elastic modulus by considering strain and stress throughout the crystal, respectively. The arithmetic mean of these two obtained limits is also found by Hill approximation (H) [51]. Accordingly, calculations are made using the following equations [49-51]:

$$B_V = (1/9)[C_{11} + C_{22} + C_{33} + 2(C_{12} + C_{13} + C_{23})]$$

$$B_R = \Delta[C_{11}(C_{22} + C_{33} - 2C_{23}) + C_{22}(C_{33} - 2C_{13}) - 2C_{33}C_{12} + C_{12}(2C_{23} - C_{12}) + C_{13}(2C_{12} - C_{13}) + C_{23}(2C_{13} - C_{23})]^{-1}$$

$$G_V = (1/15)[C_{11} + C_{22} + C_{33} + 3(C_{44} + C_{55} + C_{66}) - (C_{12} + C_{13} + C_{23})]$$

$$G_R = 15\{4[C_{11}(C_{22} + C_{33} + C_{23}) + C_{22}(C_{33} + C_{13}) + C_{33}C_{12} - C_{12}(C_{23} + C_{12}) - C_{13}(C_{12} + C_{13}) - C_{23}(C_{13} + C_{23})]/\Delta + 3[(1/C_{44}) + (1/C_{55}) + (1/C_{66})]\}^{-1}$$

$$\Delta = C_{13}(C_{12}C_{23} - C_{13}C_{22}) + C_{23}(C_{12}C_{13} - C_{23}C_{11}) + C_{33}(C_{11}C_{22} - C_{12}^2)$$

$$G_H = (G_V + G_R)/2$$

$$B_H = (B_V + B_R)/2.$$

Table 5. The equilibrium B_V , B_R , B_H , G_V , G_R , G_H (G the), ratio of B_H/G_H , ν , and H_V (GPa) for WP under different pressure with available experimental and theoretical values at 0 GPa

Pressure (GPa)	B_V	B_R	B_H	G_V	G_R	G_H	B_H/G_H	E	ν	H_V
0	237.02	223.96	230.49	126.93	117.90	122.41	1.88	312.00	0.27	13.5
0 (Exp.) [26]			223.37							
0 (Theo.) [47, 48]			221.55			117.47	1.89	299.47	0.27	
10	275.99	260.18	268.09	144.11	134.24	139.17	1.93	355.92	0.28	14.4
20	311.75	294.02	302.88	159.23	148.77	154.01	1.97	395.06	0.28	15.1
30	345.26	326.14	335.70	173.16	162.37	167.76	2.00	431.43	0.29	15.7
40	377.05	356.56	366.81	185.71	174.62	180.16	2.04	464.45	0.29	16.2
50	407.45	385.51	396.48	196.90	185.45	191.17	2.07	494.10	0.29	16.6

The B_H indicates the ability of materials against changes in volume, while the G_H shows the resistance of materials to shape change [52, 53]. Our calculated values of B_V , B_R , B_H , G_V , G_R , and G_H under pressure are represented in Table 5 with the previously reported values [26, 47, 48]. It is observed that our calculated values are close to the available results. The variations of normalized B_H and G_H with increasing pressure are also plotted in Figure 3. As seen from the results, all three important quantities are increased monotonically with enhancing pressure. Additionally, higher values of volume and shear modulus indicate that their deformations are so strong [52, 54]. B_H has a higher deviation than others under pressure. When we analyze the B_H/G_H ratio, which can be calculated to find the brittle or ductile nature of materials using Pugh's theory [52], we easily determine the mechanical properties of this compound. According to Pugh's theory, when B_H/G_H ratio is higher than 1.75, the material has ductile behavior; otherwise, it has brittle behavior [52, 55, 56]. The calculated B_H/G_H ratio of WP compound with different pressure are given in Table 5. It is found that the WP exhibits ductile behavior and it has the best ductility at 50 GPa.

Besides these properties, using the calculated B_H and G_H , Young's modulus E and Poisson's ratio ν can be computed with the equations given below [57]:

$$E = \frac{9B_H G_H}{3B_H + G_H}, \quad \nu = \frac{3B_H - 2G_H}{2(3B_H + G_H)}.$$

The values of E and ν calculated by giving different pressures are summarized in Table 5. Young's modulus indicates the measure of stiffness in materials [54]. The change in Young's modulus concerning pressure is plotted in Figure 3. It is clear that the values of Young's modulus increase with the increase in pressure. Furthermore, the brittle or ductile behavior of materials is found with Poisson's ratio [58]. If ν is greater than 0.26, then ductile behavior is defined; otherwise, materials show a brittle behavior [59, 60]. It means that the larger value of ν indicates better plasticity. When we increase the pressure from 0 GPa to 50 GPa, ν for WP is enhanced from 0.27 to 0.29. According to these results, the WP compound becomes more ductile when increasing pressure. If you want to obtain information about the bond strengths in the compound, the Poisson's ratio can be calculated. It is known that the ν value is given as 0.1 and 0.25 for covalent materials (brittle) and ionic materials (ductile), respectively [61]. These results show that the contribution of ionic bonds to atomic bonding dominates the WP compound. Another method of estimating the brittle or ductile form of materials is to find Cauchy's pressure. Cauchy's pressure can be defined by $(C_{23} - C_{44})$, $(C_{13} - C_{55})$, and $(C_{12} - C_{66})$ for the (100), (010), and (001) planes, respectively [62]. Cauchy pressure gives information about the angular character of atomic bonds in materials [52, 55, 63]. When the

Cauchy pressure is a positive value, the material shows a metallic bonding character. However, the negative value shows covalent bonding and angular character [64, 65]. While it is found that the positive results for $(C_{23} - C_{44})$ and $(C_{13} - C_{55})$, the negative results are evaluated for $(C_{12} - C_{66})$ for our calculations. It is indicated that the bonding in the (100) and (010) planes has a metallic character, whereas the (001) planes have an angular character. The degree of resistance to elastic or plastic deformation for a solid material is determined by its Vickers hardness. We have calculated the Vickers hardness of WP under pressure. The equation suggested by Tian et al. [66] for calculating the hardness of the material is given as

$$H_V = 0.92 k^{1.137} G^{0.708}$$

where $k = G_H/B_H$ and G_H is the shear modulus. The calculated hardness of WP under pressure is given in Table 5. The hardness of WP increase with the increasing pressure. The greater the hardness the stronger the bond strength (W-P). The hardness values calculated for WP are consistent with the change of elastic modulus. Plastic deformation and elastic instability can be affected by elastic anisotropy. For this reason, elastic anisotropy of WP is investigated under different pressure values. The universal anisotropic index A^U and percent anisotropy A_B and A_G are computed using the given equations [67]:

$$A^U = 5 \frac{G_V}{G_R} + \frac{B_V}{B_R} - 6 \geq 0$$

$$A_B = \frac{B_V - B_R}{B_V + B_R}$$

$$A_G = \frac{G_V - G_R}{G_V + G_R}$$

Our calculated anisotropic indexes are given in Table 6. If these values are equal to zero, it shows elastic isotropy, if not, it is anisotropic elastic property. A_B and A_G values are almost the same which means that the WP compound studied under different pressure values shows the same strength or weakness in the bulk modulus and shear modulus. In addition, the higher the A^U value, the stronger the anisotropic elastic property of the material. Our calculated A^U values under different pressures are almost the same.

Table 6. The calculated A^U , A_B and A_G for WP under different pressure

Pressure (GPa)	A^U	A_B	A_G
0	0.4411	0.0283	0.0369
10	0.4284	0.0295	0.0355
20	0.4118	0.0293	0.0340
30	0.3907	0.0285	0.0321
40	0.3749	0.0279	0.0308
50	0.3655	0.0277	0.0299

Going further, after investigating the mechanical properties, we have focused on the electronic properties of the WP compound. Electronic properties of materials ensure essential information to define the bonding nature of a crystal and related properties. Electronic properties are important for understanding the structure. This can also be affected by the pressure. The electronic band structures of WP for pressures for 0 GPa 50 GPa are calculated, as seen in Figures 4(a) and (b). Our results show that WP has a metallic character because of the valence and conduction bands crossing the Fermi energy level. Our calculated electronic band structure for 0 GPa is consistent with available theoretical results [3, 9, 25, 26]. The metallic structure of WP is preserved with the increase in pressure.

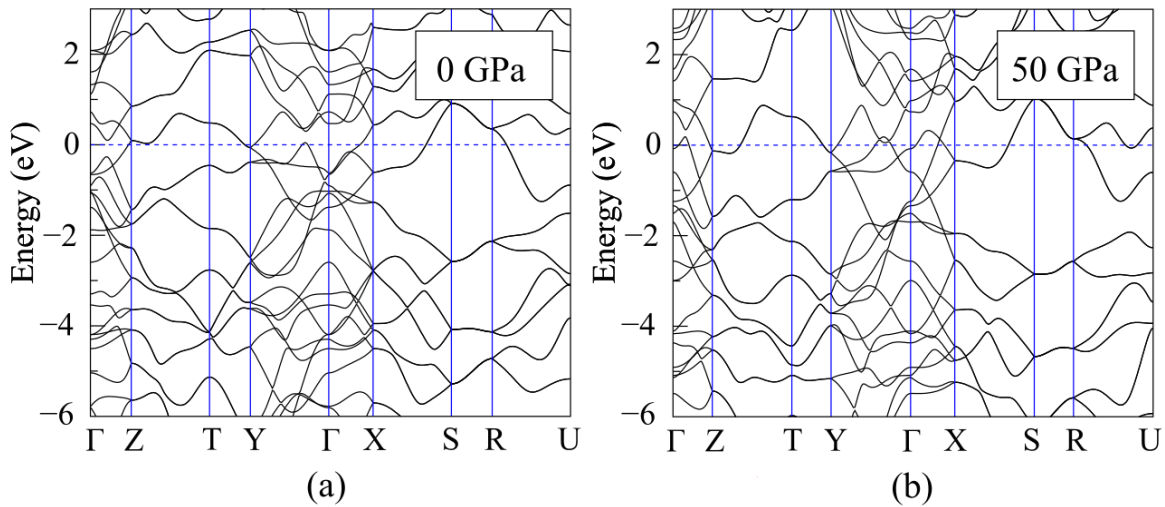


Figure 4. The calculated electronic band structures for WP under pressure at (a) 0 GPa, and (b) 50 GPa. The Fermi level is set to zero

Interestingly, there is the only difference in the band structure between Y- Γ and Γ -X symmetry points above the Fermi level. Indeed, some bands are shifted up around the Fermi Level for these symmetry points with increasing pressure. Besides, to ensure more details about the electronic properties, we have further calculated the total (TDOS) and partial density of states (PDOS) as plotted in Figures 5(a) and (b) for 0 GPa and 50 GPa, respectively. When the two situations given in Figure 5 are examined the lowest energy region of the valence band is described by the s -orbital of P atoms and the small contribution of W- d orbitals, W- p orbitals, W- s orbitals, and P- p orbitals, respectively. It is seen clearly that the states mainly contributed from W- d orbitals above -8 eV. There is a hybridization between W- d and orbitals P- p orbitals below the Fermi level between -8 eV and -2 eV. There is no significant change in DOS and PDOS in the considered pressures. It is only concluded that the states pushed to the lower energies, enhancing pressure. Our calculated band structures, TDOS and PDOS, are consistent with previous theoretical studies [3, 9, 25, 26, 68].

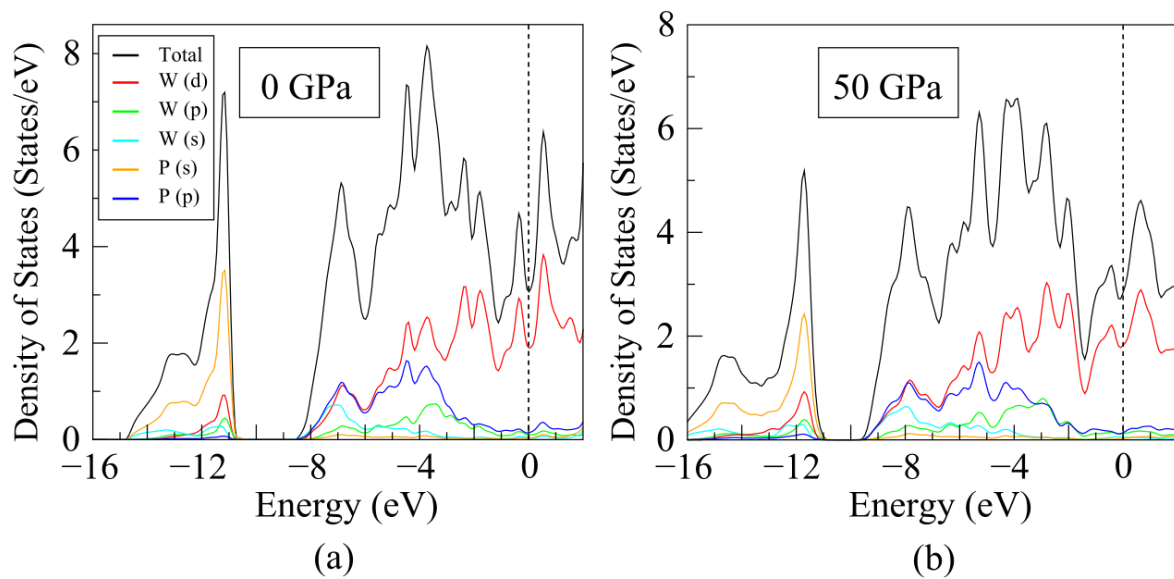


Figure 5. TDOS and PDOS of WP for (a) 0 GPa, and (b) 50 GPa pressures. The Fermi level is set to zero

4. RESULTS

As a consequence, the structural, mechanical, electronic and dynamic properties of WP compound have been investigated using DFT method under increasing pressure values. Structural parameters calculated in this study, such as lattice constant, volume and bond length, are compatible with previously found results. The normalized structural parameters are decreased with the enhancing pressure (0-50 GPa). The elastic constants and mechanical properties are calculated to discuss mechanical stability, they show that the values of elastic constants and mechanical properties enhance with increasing pressure. The computed properties show that WP is the ductile phase. The calculated hardness value of WP using the bulk modulus and shear modulus has a slightly higher value under 50 GPa than at other pressures. For all pressures, the calculated electronic band structure shows that WP indicates metallic behavior. We have also found that W-*d* orbital is dominated at all pressures. Finally, it is found that WP is dynamically stable over the 0 GPa-50 GPa pressure range.

ACKNOWLEDGMENTS

This study was supported by T.C. Strategy and Budget Directorate the project numbered 2019K1292587.

CONFLICTS OF INTEREST

No conflict of interest was declared by the authors.

REFERENCES

- [1] Rundqvist S., "Phosphides of the B31 (MnP) Structure Type", *Acta Chemica Scandinavica*, 16: 287-292, (1962).
- [2] Rundqvist S., Lundström, T. "X-Ray Studies of Molybdenum and Tungsten Phosphides", *Acta Chemica Scandinavica*, 17: 37-46, (1963).

- [3] Joshi, R., Sahariya, J., Mund, H.S., Bhamu, K.C., Tiwari, S., Ahuja B.L., “Compton profiles of MoP and WP: Validation of second-order generalized gradient approximation”, *Computational Materials Science*, 53(1): 89-93, (2012).
- [4] Wu, W, Cheng, J.-G., Matsubayashi, K., Kong, P., Lin, F., Jin C., Wang, N., Uwatoko, Y., Luo, J., “Superconductivity in the vicinity of antiferromagnetic order in CrAs”, *Nature Communications*, 5: 5508, (2014).
- [5] Kotegawa, H., Nakahara, S., Tou, H., Sugawara, H. “Superconductivity of 2.2 K under Pressure in Helimagnet CrAs”, *Journal of the Physical Society of Japan*, 83: 093702, (2014).
- [6] Kotegawa, H., Nakahara, Akamatsu, R., Tou, H., Sugawara, H., Harima, H., “Detection of an Unconventional Superconducting Phase in the Vicinity of the Strong First-Order Magnetic Transition in CrAs Using ⁷⁵As-Nuclear Quadrupole Resonance”, *Physical Review Letters*, 114: 117002, (2015).
- [7] Cheng, J.-G., Matsubayashi, K., Wu, W., Sun, J. P., Lin, F. K., Luo, J. L., Uwatoko, Y., “Pressure-Induced Superconductivity on the border of Magnetic Order in MnP”, *Physical Review Letters*, 114: 117001, (2015).
- [8] Liu, Z., Wu, W., Zhao, Z., Zhao, H., Cui, J., Shan, P., Zhang, J., Yang, C., Sun, P., Wei, Y., Li, S., Zhao, J., Sui, Y., Cheng, J., Lu, L., Liu, G., Superconductivity in WP single crystals”, *Physical Review B*, 99: 184509, (2019).
- [9] Cuono G., Forte, F., Cuoco, M., Islam, R., Luo, J., Noce C., Autieri, C., “Multiple band crossings and Fermi surface topology: Role of double nonsymmorphic symmetries in MnP-type crystal structures”, *Physical Review Materials*, 3(9): 095004, (2019).
- [10] Wu, W., Cheng, L., Matsubayashi, K., Kong, P., Lin, F., Jin, C., Wang, N., Uwatoko, Y., Luo, J., “Superconductivity in the vicinity of antiferromagnetic order in CrAs”, *Nature Communications*, 5: 5508, (2014).
- [11] Chen R. Y., Wang, N. L., “Progress in Cr- and Mn-based superconductors: a key issues review”, *Reports on Progress in Physics*, 82: 012503, (2019).
- [12] Wang, Y., Feng, Y., Cheng, J.-G., Wu, W., Luo, J. L., Rosenbaum, T. F., “Spiral magnetic order and pressure-induced superconductivity in transition metal compounds”, *Nature Communications*, 7: 13037, (2016).
- [13] Autieri C., Noce, C., “First-principles study of structural, magnetic and electronic properties of CrAs”, *Philosophical Magazine*, 97: 3276, (2017).
- [14] Autieri, C., Cuono, G., Forte, F., Noce, C., “Low energy bands and transport properties of chromium arsenide”, *Journal of Physics: Condensed Matter*, 29: 224004, (2017).
- [15] Motizuki, K., Ido, H., Itoh, T., Morifuji, M., “Electronic Structure and Magnetism of 3d-Transition Metal Pnictides”, *Springer Series in Materials Science (Springer-Verlag, Berlin)* (2010).
- [16] Roberts, B. W., “Superconductive Materials and Some of Their Properties (National Bureau of Standards)”, Washington, DC, (1969).
- [17] Guerin, R., Jacques, M., Prigent, J., “Etude des chaines metal-metal dans la structure type MnP: Les arseniure et phosphure “MoAs” et WP et leurs solutions solides avec) les composes MX (M = élément de transition 3d; X = As, P)”, *Materials Research Bulletin*, 10(9): 957-965, (1975).

- [18] Kandler, H., Reiss, B., Naturforschg, Z., “Zur Kristallstruktur der intermetallischen Phasen MoAs und Mo₅As”, Zeitschrift für Naturforschung, 21a: 549-554, (1966).
- [19] Fjellvåg, H., Selte, K., Danihelka, P., “Structural and Magnetic Properties of Mn_(1-t)Mo_(t)As”, Acta Chemica Scandinavica, A38: 789–794, (1984).
- [20] Faller, F.E., Biltz W., Meisel, K., Zumbusch, M.Z., “Beiträge zur systematischen Verwandtschaftslehre. 99. Über Phosphide von Wolfram, Molybdän und Chrom”, Zeitschrift für anorganische und allgemeine Chemie, 248: 209, (1941).
- [21] Schönberg, N., “An X-Ray Investigation of Transition Metal Phosphides”, Acta Chemica Scandinavica, 8: 226-239, (1954).
- [22] Bachmayer, K., Nowotny, H., Kohl, A., “Die Struktur von TiAs”, Physikalische, Anorganische und Analytische Chemie, 86: 39-43, (1955).
- [23] Gopalakrishnan, J., Pandey, S., Rangan, K. K., “Convenient Route for the Synthesis of Transition-Metal Pnictides by Direct Reduction of Phosphate, Arsenate, and Antimonate Precursors”, Chemistry of Materials, 9(10): 2113-2116, (1997).
- [24] Lesnyak V.V., Stratiichuk D.A., Sudavtsova V.S., Slobodyanik S., “Preparation of Al, Cr, Nb, Mo, and W Monophosphides from a Lithium Metaphosphate Melt”, Russian Journal of Applied Chemistry, 74(8): 1274–1277, (2001).
- [25] Jaiganesh R., Eithiraj D., Kalpana, G., “Theoretical study of electronic, magnetic and structural properties of Mo and W based group V (N, P, As, Sb and Bi) compounds”, Computational Materials Science, 49(1): 112-120, (2010).
- [26] Tayran, C., Çakmak, M., “Electronic structure, phonon and superconductivity for WP 5d-transition metal”, Journal of Applied Physics, 126: 175103, (2019).
- [27] Kresse, G., Hafner, J., “Ab initio molecular dynamics for liquid metals”, Physical Review B, 47: 558(R), (1993).
- [28] Kresse, G., Furthmüller J., “Efficiency of ab-initio total-energy calculations for metals and semiconductors using a plane-wave basis set”, Computational Materials Science, 6: 15, (1996).
- [29] Kresse, G., Joubert, D., “From ultrasoft pseudopotentials to the projector augmented-wave method”, Physical Review B, 59: 1758, (1999).
- [30] Perdew, J.P., Burke, K., Ernzerhof, M., “Generalized Gradient Approximation Made Simple”, Physical Review Letters, 77: 3865-3868, (1994). [Erratum Phys. Rev. Lett. 78, 1396 (1997)].
- [31] Blöchl, P.E., “Projector augmented-wave method”, Physical Review B, 50: 17953, (1994).
- [32] Kresse, G., Furthmüller J., “Efficient iterative schemes for ab initio total-energy calculations using a plane-wave basis set”, Physical Review B, 54: 11169, (1996).
- [33] Monkhorst, H.J., Pack, J.D., “Special points for Brillouin-zone integrations”, Physical Review B, 13: 5188, (1976).
- [34] Momma, K., Izumi, F., “VESTA 3 for three-dimensional visualization of crystal, volumetric and morphology data”, Journal of Applied Crystallography, 44: 1272-1276, (2011).

- [35] Togo, A., Tanaka I., “First principles phonon calculations in materials science”, *Scripta Materialia*, 108: 1-5, (2015).
- [36] Kanaya, K., Abe, S., Yoshida, H., Kamigaki, K., Kaneko, T., “Magnetic and structural properties of pseudo-binary compounds $\text{CrAs}_{1-x}\text{Px}$ ”, *Journal of Alloys and Compounds*, 383: 189, (2004).
- [37] Niu, Q., Yu, W. C., Yip, K. Y., Lim, Z. L., Kotegawa, H., Matsuoka, E., Sugawara, H., Tou, H., Yanase, Y., Goh, S.K., “Quasilinear quantum magnetoresistance in pressure-induced nonsymmorphic superconductor chromium arsenide”, *Nature Communications*, 8: 15358, (2017).
- [38] Ashcroft, N.W., Mermin, N.D., “Solid State Physics”, Saunders, Philadelphia, (1976).
- [39] Sailuam W., Phacheerak, K., Bootchanont, A., Fongkaew, I., Limpijumnong S., “Elastic and mechanical properties of hydroxyapatite under pressure: A first-principles investigation”, *Computational Condensed Matter*, 24: e00481, (2020).
- [40] Ravindran, P., Fast, L., Korzhavyi, P.A., Johnsson, B., Wills, J., Eriksson, O., “Density functional theory for calculation of elastic properties of orthorhombic crystals: Application to TiSi_2 ”, *Journal of Applied Physics*, 84(9): 4891, (1998).
- [41] Mattesini M., Matar, S.F., “Density-functional theory investigation of hardness, stability, and electron-energy-loss spectra of carbon nitrides with C_{11}N_4 stoichiometry”, *Physical Review B*, 65: 075110, (2002).
- [42] Wu, Z.J., Zhao, E.J., Xiang, H.P., Hao, X.F., Liu X.J., Meng, J., “Crystal structures and elastic properties of superhard IrN_2 and IrN_3 from first principles”, *Physical Review B*, 76: 054115, (2007).
- [43] Birch F., “Finite Elastic Strain of Cubic Crystals”, *Physical Review*, 71: 809, (1947).
- [44] M. Born, K. Huang, “Dynamical Theory of Crystal Lattices”, Clarendon, Oxford, 1956.
- [45] Beckstein, O., Klepeis, J.E., Hart, G.L.W., Pankratov O., “First-principles elastic constants and electronic structure of $\alpha\text{-Pt}_2\text{Si}$ and PtSi ”, *Physical Review B*, 63: 134112, (2001).
- [46] Wallace D.C., “Thermodynamics of Crystals”, Wiley, New York (Chap. 1), (1972).
- [47] Jong, M. de, Chen, W., Angsten, T., Jain, A., Notestine, R., Gamst, A., Sluiter, M., Krishna Ande, C., Zwaag, S. van der, Plata, J. J., Toher, C., Curtarolo, S., Ceder, G., Persson, K. A., Asta, M., “Charting the complete elastic properties of inorganic crystalline compounds”, *Scientific Data*, 2: 150009, (2015).
- [48] [Gaillac, R., Pullumbi, P., Coudert, F.-X., “ELATE: an open-source online application for analysis and visualization of elastic tensors”, *Journal of Physics-Condensed Matter*, 28: 275201, (2016).
- [49] Voigt, W., “Lehrbuch der Kristallphysik (mit Ausschluss der Kristalloptik)”, Teubner, Leipzig, (1928).
- [50] Reuss A., “Berechnung der Fließgrenze von Mischkristallen auf Grund der Plastizitätsbedingung für Einkristalle”, *ZAMM-Journal of Applied Mathematics and Mechanics/Zeitschrift für Angewandte Mathematik und Mechanik*, 9: 49-58, (1929).
- [51] Hill, R., “The Elastic Behaviour of a Crystalline Aggregate”, *Proceedings of the Physical Society*, 65(5): 349–354, (1952).

- [52] Pugh, S. F., "XCII. Relations between the elastic moduli and the plastic properties of polycrystalline pure metals", *Philosophical Magazine*, 45: 823-843, (1954).
- [53] Young, A. F., Sanloup, C., Gregoryanz, E., Scandolo, S., Hemley, R. J., Mao, H. K., "Synthesis of Novel Transition Metal Nitrides IrN_2 and OsN_2 ", *Physical Review Letters*. 96(15): 155501, (2006).
- [54] Yang, X., Hao, A., Wang, X., Liu, X., Zhu, Y., "First-principles study of structural stabilities, electronic and elastic properties of BaF_2 under high pressure", *Computational Materials Science*, 49: 530-534, (2010).
- [55] Pettifor, D.G., "Theoretical predictions of structure and related properties of intermetallics", *Materials Science and Technology*, 8(4): 345-349, (1992).
- [56] Chen, H., Lei, X., Long, J., Huang, W., "The elastic and thermodynamic properties of new antiperovskite-type superconductor CuNNi_3 under pressure", *Materials Science in Semiconductor Processing*, 27: 207-211, (2014).
- [57] Wu, Z. J., Zhao, E. J., Xiang, H. P., Hao, X. F., Liu, X. J., Meng, J., "Crystal structures and elastic properties of superhard IrN_2 and IrN_3 from first principles", *Physical Review B*, 76: 054115, (2007).
- [58] Yang, R., Zhu, C., Wei, Q., Du, Z., "Investigations on structural, elastic, thermodynamic and electronic properties of TiN , Ti_2N and Ti_3N_2 under high pressure by first-principles", *Journal of Physics Chemistry of Solids*, 98: 10-19, (2016).
- [59] Haines, J., Léger, J., Bocquillon, G., "Synthesis and Design of Superhard Materials", *Annual Review of Materials Research*, 31: 1-23, (2001).
- [60] Qi, C., Jiang, Y., Liu, Y., Zhou, R., "Elastic and electronic properties of XB_2 ($\text{X}=\text{V}, \text{Nb}, \text{Ta}, \text{Cr}, \text{Mo}$, and W) with AIB_2 structure from first-principles calculations", *Ceramics International*, 40(4): 5843-5851, (2014).
- [61] Kanoun, M.B., Goumri-Said, S., Reshak, A.H., Merad, A.E., "Electro-structural correlations, elastic and optical properties among the nanolaminated ternary carbides Zr_2AC ", *Solid State Science*, 12(5): 887-898, (2010).
- [62] Wen, Y., Wang, L., Liu, H., Song, L., "Ab Initio Study of the Elastic and Mechanical Properties of B_{19}TiAl ", *Crystals*, 7: 39, (2017).
- [63] Papadimitriou, I., Utton, C., Scott, A., Tsakirooulos, P., "Ab Initio Study of Binary and Ternary $\text{Nb}_3(\text{X}, \text{Y})\text{A}_{15}$ Intermetallic Phases ($\text{X}, \text{Y} = \text{Al}, \text{Ge}, \text{Si}, \text{Sn}$)", *Metallurgical and Materials Transactions A*, 46(2): 566-576, (2015).
- [64] Abadias, G., Kanoun, M.B., Goumri-Said, S., Koutsokeras, L., Dub, S.N., Djemia, Ph., "Electronic structure and mechanical properties of ternary ZrTaN alloys studied by ab initio calculations and thin-film growth experiments", *Physical Review B*, 90: 144107, (2014).
- [65] Chen, H., Lei, X., Long, J., Huang, W., "The elastic and thermodynamic properties of new antiperovskite-type superconductor CuNNi_3 under pressure", *Materials Science in Semiconductor Processing*, 27: 207-211, (2014).
- [66] Tian, Y.J. Xu, B., Zhao, Z.S., "Microscopic theory of hardness and design of novel superhard crystals", *International Journal of Refractory Metals and Hard Materials*, 33: 93-106 (2012).

- [67] Chen, X.Q., Fu, C.L., Krčmar, M., “Electronic and Structural Origin of Ultraincompressibility of 5d Transition-Metal Diborides MB_2 (M=W, Re, Os)”, 100: 196403 (2008).
- [68] Jain, A., Ong, S. P., Hautier, G., Chen, W., Richards, W. D., Dacek, S., Cholia, S., Gunter, D., Skinner, D., Ceder, G., Persson, K. A., “Commentary: The Materials Project: A materials genome approach to accelerating materials innovation”, APL Materials, 1: 011002, (2013).